

# Comparison of Physical Realizations of Multidimensional Voronoi Constellations in Single Mode Fibers

Ali Mirani<sup>(1)</sup>, Kovendhan Vijayan<sup>(1)</sup>, Shen Li<sup>(2)</sup>, Zonglong He<sup>(1)</sup>,  
Jochen Schröder<sup>(1)</sup>, Peter Andrekson<sup>(1)</sup>, Erik Agrell<sup>(2)</sup>, Magnus Karlsson<sup>(1)</sup>

<sup>(1)</sup> Photonics Laboratory, Department of Microtechnology and Nanoscience, Chalmers University of Technology, Gothenburg, Sweden, [mirani@chalmers.se](mailto:mirani@chalmers.se)

<sup>(2)</sup> Department of Electrical Engineering, Chalmers University of Technology, Gothenburg, Sweden

**Abstract** We investigate experimentally and numerically the impact of using different fiber dimensions to spread out the 32-dimensional Voronoi constellations. We find similar performance in experiments and less than 5.4% reach improvements in long-haul transmission simulations by spreading the constellation dimensions over time slots compared to wavelengths. ©2022 The Author(s)

## Introduction

Geometric and probabilistic constellation shaping are used to close the 1.53 dB shaping gap to the Shannon limit<sup>[1]</sup>. Probabilistic shaping has the advantage of rate adaptability while increasing the complexity and latency of the system with a distribution matcher<sup>[2]</sup>. On the other hand, geometric shaping (GS) is usually used in fixed rates and can be designed for either linear or nonlinear channels as well as adapted to different impairments<sup>[3]</sup>. For instance, in<sup>[4]</sup>, constellations are geometrically designed to tolerate laser phase noise. In the presence of transceiver impairments, end-to-end learning was applied in<sup>[5]</sup> to design geometrically shaped constellations. In<sup>[6],[7]</sup>, 4-dimensional constellations are optimized in a multi-span nonlinear fiber channel.

The Voronoi constellations (VC) based on multidimensional lattices are a type of GS with low-complexity encoding and decoding algorithms without look-up tables to store the constellation symbols<sup>[8]</sup>. In contrast to many other geometrically shaped constellations, increasing the constellation size or spectral efficiency (SE) does not add algorithmic complexity. VCs have been studied for the additive white Gaussian noise (AWGN) channel<sup>[9],[10]</sup>, single wavelength and polarization<sup>[11]</sup>, or multiple wavelengths and polarizations systems<sup>[12]</sup>. However, different physical realizations of VCs over the available dimensions of standard single mode fibers have not been compared.

In this work, we compare different physical realizations of 32-dimensional VCs with SEs of 1 and 2 bits/symbol/dimension. These modulation formats are simulated for both the AWGN and nonlinear fiber channels, and experimentally investigated in multiple time slots, wavelengths, and polarizations in the presence of transceiver and fiber channel impairments. We experimentally show that

when the transmitted signal is dominated by the noise from the optical amplifier, there is a similar performance between spreading the physical dimensions over wavelengths or polarizations compared to time slots. Furthermore, in the long-haul transmission simulations without transceiver impairments, we show almost 0 and 5.4% reach improvements when the constellations dimensions are spread from 8 wavelengths to 8 time slots at SEs of 1 and 2 bits/symbol/dimension, respectively.

## Voronoi constellation realizations

In this work, we consider two 32-dimensional Voronoi constellations based on the first-order Reed-Muller code<sup>[9]</sup> with SEs of 1 (BW32B1) and 2 (BW32B2) bits/symbol/dimension and constellation sizes of  $2^{32}$  and  $2^{64}$ , respectively. The bit-to-symbol mapping and symbol-to-bit demapping algorithms are described in<sup>[8],[13],[14]</sup>.

In order to transmit the multidimensional VCs over physical fiber dimensions, we convert the 32-dimensional real symbols into multiple complex numbers to modulate the amplitude and phase (in-phase and quadrature (I/Q) components) in different sets of time slots (ts), polarizations (pol), or wavelengths (wl). We use the frame structure in<sup>[15]</sup> for the I/Q components in each polarization and wavelength.

In the receiver, after detecting all physical dimensions and offline pilot-aided signal processing<sup>[16]</sup>, we convert the complex numbers into real multidimensional symbols and apply the closest point algorithm based on decoding unions of cosets<sup>[17]</sup> to estimate the transmitted symbols and calculate the bit error rate (BER). The quadrature amplitude modulation (QAM) formats with Gray labeling and maximum likelihood detection are used as a benchmark to compare the performance of

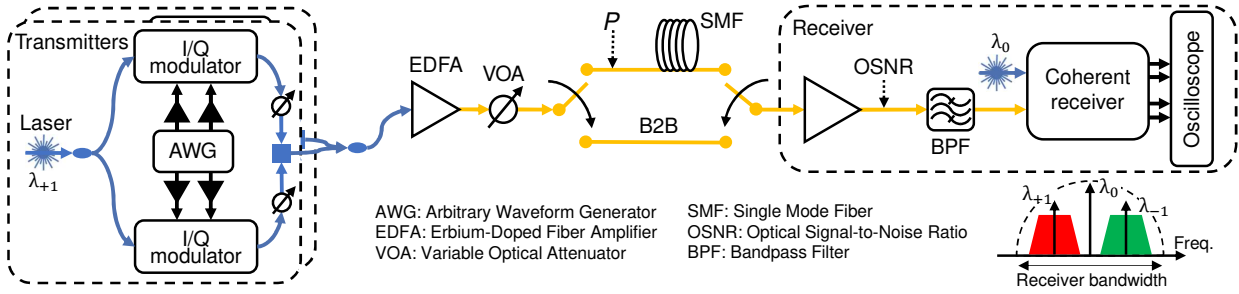


Fig. 1: Experimental setup with two transmitters and a single coherent receiver to detect two wavelengths simultaneously.

VCs at the same SE.

### Simulation and experimental setups

We perform simulations for both the AWGN channel and a long-haul transmission link. In the long-haul transmission simulations, we solve the nonlinear Schrödinger equation (NLSE) numerically using the Manakov equation<sup>[18]</sup> and split-step Fourier method<sup>[19]</sup> to model the transmission in a fiber with 0.2 dB/km attenuation, 16.8 ps/nm/km dispersion, and  $1.3 \text{ (W km)}^{-1}$  nonlinearity. Each span of fiber is 80 km and it is followed by an erbium-doped fiber amplifier (EDFA) with 5 dB noise figure and a gain equivalent to the span loss. The dispersion is only compensated at the receiver side.

The experimental setup is shown in fig. 1. The optical carriers generated from two independent external cavity lasers (ECLs) of linewidths  $\leq 100$  kHz operating at 1550.16 nm and 1550.26 nm are split up into two arms by 3 dB couplers. Each arm is modulated by an I/Q mod-

ulator driven by amplified electrical signals from an arbitrary waveform generator (AWG) with a 10 Gbaud signal. A variable optical attenuator (VOA) after each I/Q modulator is used to balance or block the power of the arms. For each wavelength, the output of the VOAs are combined using a polarization beam combiner to create a dual-polarization (DP) signal. The modulated wavelengths are then combined with a 3 dB coupler and amplified with a booster EDFA. A VOA is used to sweep the power into the pre-amplifier changing the optical signal-to-noise ratio (OSNR) for noise loading and to set the required launch power,  $P$ , at the transmission span input in case of the fiber transmission. The OSNR is defined over 0.1 nm bandwidth and it is normalized per wavelength and polarization for all of the experiments. The fiber and EDFA parameters are approximately similar to the long-haul transmission simulation parameters.

On the receiver side, the signal is pre-amplified and filtered to remove the out-of-band noise. It is then fed into a coherent receiver with 22 GHz

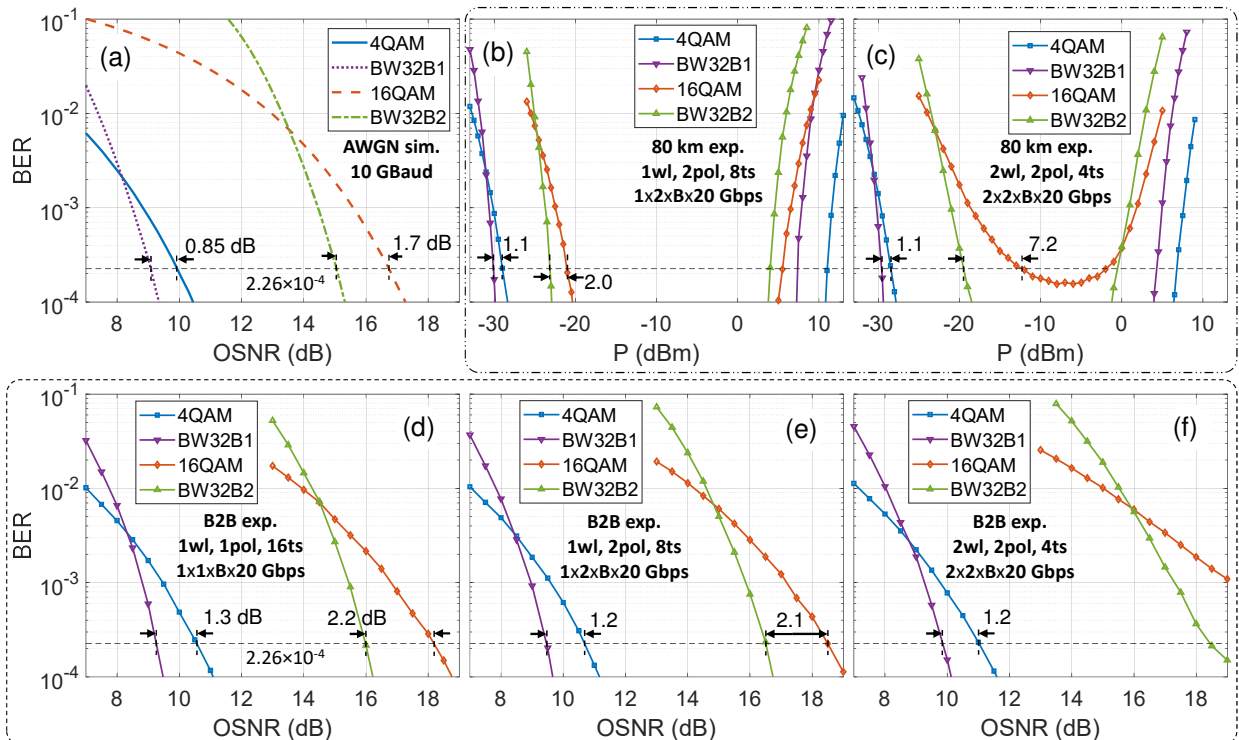
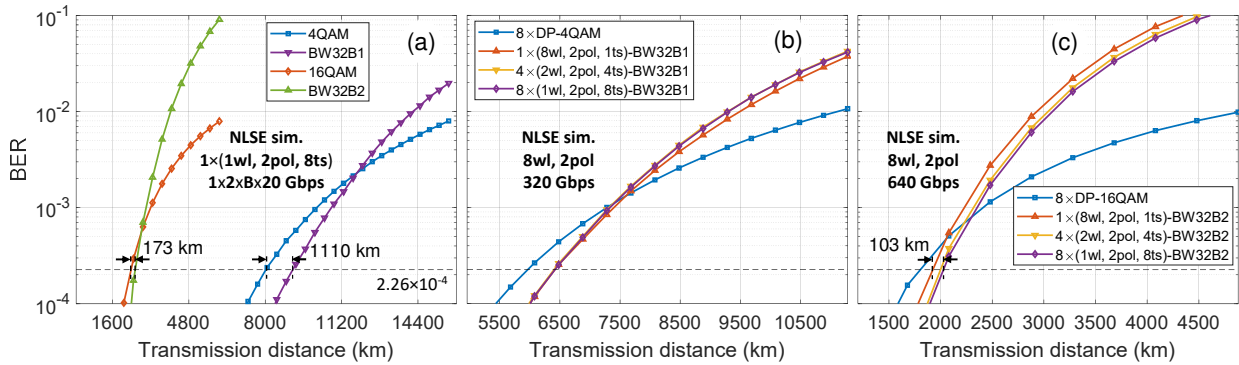


Fig. 2: The BER performance in (a) AWGN simulation, (b), (c) single span transmission experiment, and (d), (e), (f) back-to-back experiment. The OSNR and  $P$  are measured over the total signals bandwidth, then normalized per wavelength and polarization.



**Fig. 3:** The BER at the optimum optical launch power performance in long-haul single mode fiber transmission simulation. (a) Single wavelength simulation, (b), (c) comparison of different realization occupying 8 wavelengths and 2 polarizations.

small-signal bandwidth. A free-running ECL with  $\leq 100$  kHz linewidth is used as local oscillator for both channels at their average wavelength 1550.21 nm. The electrical signals from the coherent receiver are sampled using a real-time oscilloscope and processed offline to compensate for channel and receiver impairments.

### Results and discussions

We compare the uncoded BER performance of VCs with regular QAM formats at the same SEs both in simulation and experiment.

In fig. 2(a), modulation formats are simulated for the AWGN channel. There is a crossing point where for lower BERs, VCs outperform QAM formats. At the hard-decision forward error correction (HD-FEC) threshold<sup>[20]</sup> of  $\text{BER} = 2.26 \times 10^{-4}$ , the OSNR improvement for VCs are 0.85 and 1.7 dB at SEs of 1 and 2 bits/symbol/dimension, respectively. Fig. 2(a) can be used to measure the implementation penalties for different realizations over physical fiber dimensions. For instance, in fig. 2(d), using 1 wavelength, 1 polarization, and 16 time slots to implement a 32-dimensional space, the implementation penalties are approximately 0.65, 0.4, 1.45, and 0.95 dB for 4QAM, BW32B1, 16QAM, and BW32B2, respectively, at the HD-FEC threshold. Comparing the simulation and experiment, the reasons for higher OSNR improvements in fig. 2(d, e, f) than fig. 2(a) at low BERs are the enhanced sensitivity and lower implementation penalties of VCs compared to QAM formats. Furthermore, by spreading over other physical dimensions than time slots, the implementation penalty increases due to the differences in performance of transceiver components. Moreover, the OSNR improvement of VCs compared to QAM formats decreases slightly by spreading the dimensions from time slots to wavelengths and polarizations as shown in fig. 2(d, e, f).

Fig. 2(b, c) show the results of a single-span transmission in 1 and 2 wavelengths experiment, respectively, where both transceiver and fiber im-

pairments arise. Due to the dual-wavelength detection with a single coherent receiver in fig. 2(c) (similar to fig. 2(f)), we see that the power improvement for 2 bits/symbol/dimension increases from 2.0 to 7.2 dB at the HD-FEC threshold. However, at 1 bits/symbol/dimension, there is no improvement in the optical power between different realizations.

In fig. 3, the long-haul nonlinear fiber simulations are shown as we spread the physical dimensions from time slots to wavelengths. In fig. 3(a), single wavelength simulations are shown comparing QAM formats and VCs at the same SEs. At the HD-FEC threshold, we show 173 and 1110 km reach improvements for VCs compared to QAM formats at 1 and 2 bits/symbol/dimension, respectively. In fig. 3(b, c), we compare different realizations of VCs in a long-haul transmission link with 8 wavelengths and 2 polarizations. At 1 bits/symbol/dimension in fig. 3(b), different realizations have the same reach at the HD-FEC threshold. However, fig. 3(c) shows 103 km (5.4%) reach improvement when bits are transmitted using 8 BW32B2 each spread over 8 time slots compared to 1 BW32B2 spread over 8 wavelengths.

### Conclusions

We compare different implementations of VCs over time slots, polarizations, and wavelengths in fiber simulations and experiments. We experimentally show similar performance between different realizations using time slots, wavelengths, and polarizations. Long-haul nonlinear simulations show a reach improvement of near 0 and 5.4% by spreading the VCs dimensions over time slots compared to wavelengths at 1 and 2 bits/symbol/dimension, respectively.

### Acknowledgements

This work was supported by the Knut and Alice Wallenberg Foundation, grant No. 2018.0090, and the Swedish Research Council (VR) under grant No. 2017-03702 and 2019-04078.

## References

- [1] F. Kschischang and S. Pasupathy, "Optimal nonuniform signaling for Gaussian channels", *IEEE Transactions on Information Theory*, vol. 39, no. 3, pp. 913–929, 1993. DOI: 10.1109/18.256499.
- [2] G. Böcherer, F. Steiner, and P. Schulte, "Bandwidth efficient and rate-matched low-density parity-check coded modulation", *IEEE Transactions on Communications*, vol. 63, no. 12, pp. 4651–4665, 2015. DOI: 10.1109/TCOMM.2015.2494016.
- [3] O. Vassilieva, I. Kim, H. Irie, *et al.*, "Probabilistic vs. geometric constellation shaping in commercial applications", in *Optical Fiber Communications Conference and Exhibition (OFC)*, 2022.
- [4] H. Dzieciol, G. Liga, E. Sillekens, P. Bayvel, and D. Lavery, "Geometric shaping of 2-D constellations in the presence of laser phase noise", *Journal of Lightwave Technology*, vol. 39, no. 2, pp. 481–490, 2021. DOI: 10.1109/JLT.2020.3031017.
- [5] R. T. Jones, M. P. Yankov, and D. Zibar, "End-to-end learning for GMI optimized geometric constellation shape", in *European Conference on Optical Communication (ECOC)*, 2019. DOI: 10.1049/cp.2019.0886.
- [6] B. Chen, G. Liga, Y. Lei, *et al.*, "Shaped Four-Dimensional Modulation Formats for Optical Fiber Communication Systems", in *Optical Fiber Communications Conference and Exhibition (OFC)*, 2022.
- [7] G. Liga, B. Chen, and A. Alvarado, "Model-aided geometrical shaping of dual-polarization 4D formats in the nonlinear fiber channel", in *Optical Fiber Communications Conference and Exhibition (OFC)*, 2022.
- [8] A. Mirani, E. Agrell, and M. Karlsson, "Low-complexity geometric shaping", *Journal of Lightwave Technology*, vol. 39, no. 2, pp. 363–371, 2020. DOI: 10.1109/JLT.2020.3033031.
- [9] S. Li, A. Mirani, M. Karlsson, and E. Agrell, "Low-complexity Voronoi shaping for the Gaussian channel", *IEEE Transactions on Communications*, vol. 70, no. 2, pp. 865–873, 2022. DOI: 10.1109/TCOMM.2021.3130286.
- [10] —, "Designing Voronoi constellations to minimize bit error rate", in *International Symposium on Information Theory (ISIT)*, 2021, pp. 1017–1022. DOI: 10.1109/ISIT45174.2021.9517815.
- [11] A. Mirani, K. Vijayan, Z. He, *et al.*, "Experimental demonstration of 8-dimensional Voronoi constellations with 65,536 and 16,777,216 symbols", in *European Conference on Optical Communication (ECOC)*, 2021. DOI: 10.1109/ECOC52684.2021.9605988.
- [12] A. Mirani, E. Agrell, and M. Karlsson, "Lattice-based geometric shaping", in *European Conference on Optical Communications (ECOC)*, 2020. DOI: 10.1109/ECOC48923.2020.9333162.
- [13] J. Conway and N. Sloane, "Fast quantizing and decoding and algorithms for lattice quantizers and codes", *IEEE Transactions on Information Theory*, vol. 28, no. 2, pp. 227–232, 1982. DOI: 10.1109/TIT.1982.1056484.
- [14] —, "A fast encoding method for lattice codes and quantizers", *IEEE Transactions on Information Theory*, vol. 29, no. 6, pp. 820–824, 1983. DOI: 10.1109/TIT.1983.1056761.
- [15] Y. Wakayama, T. Gerard, E. Sillekens, *et al.*, "2048-QAM transmission at 15 GBd over 100 km using geometric constellation shaping", *Opt. Express*, vol. 29, no. 12, pp. 18 743–18 759, 2021. DOI: 10.1364/OE.423361.
- [16] M. Mazur, J. Schröder, A. Lorences-Riesgo, T. Yoshida, M. Karlsson, and P. A. Andrekson, "Overhead-optimization of pilot-based digital signal processing for flexible high spectral efficiency transmission", *Opt. Express*, vol. 27, no. 17, pp. 24 654–24 669, 2019. DOI: 10.1364/OE.27.024654.
- [17] J. H. Conway and N. J. A. Sloane, *Sphere Packings, Lattices and Groups*, 3rd ed. Springer, 1999. DOI: <https://doi.org/10.1007/978-1-4757-6568-7>.
- [18] P. K. A. Wai, C. R. Menyuk, and H. H. Chen, "Stability of solitons in randomly varying birefringent fibers", *Opt. Lett.*, vol. 16, no. 16, pp. 1231–1233, 1991. DOI: 10.1364/OL.16.001231.
- [19] G. P. Agrawal, *Nonlinear Fiber Optics*, 5th ed. Springer, 2013. DOI: <https://doi.org/10.1016/C2011-0-00045-5>.
- [20] E. Agrell and M. Secondini, "Information-theoretic tools for optical communications engineers", in *IEEE Photonics Conference (IPC)*, 2018. DOI: 10.1109/IPCOn.2018.8527126.